Materials Today Physics 42 (2024) 101365

Contents lists available at ScienceDirect

Materials Today Physics

journal homepage: www.journals.elsevier.com/materials-today-physics

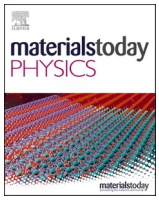

Intelligent estimation of critical current degradation in HTS tapes under repetitive overcurrent cycling for cryo-electric transportation applications

Alireza Sadeghi, Shahin Alipour Bonab, Wenjuan Song, Mohammad Yazdani-Asrami *

Propulsion, Electrification & Superconductivity Group, Autonomous Systems and Connectivity Division, James Watt School of Engineering, University of Glasgow, Glasgow, G12 8QQ, United Kingdom

ARTICLE INFO

Keywords:
Artificial intelligence
Decision tree
Fuzzy logic
Machine learning
Radial basis function
ReBCO tapes
Remaining life
Support vector machine

ABSTRACT

Overcurrent cycling refers to the procedure of imposing repetitive overcurrent to superconducting tapes/devices for characterizing their critical current reduction. Characterizing the overcurrent cycling behaviour of Rare Earth Barium Copper Oxide (ReBCO) tapes is a crucial step in the design process of High Temperature Superconducting (HTS) devices. Multiple overcurrent incidents during the operation of an HTS device can significantly decrease the total critical current, leading to potential quenches and failures. Data-driven models have been proposed in the literature to estimate the Critical Current Degradation Rate (CCDR) of ReBCO tapes under multiple overcurrent scenarios. However, these methods have exhibited notable errors in the range of 8%–11%, in the estimation of the critical current reduction. This paper proposed methods based on Artificial Intelligence (AI) techniques aimed at the challenges of conventional methods of CCDR estimation. Different AI-based techniques were proposed, tested, and compared to show the effectiveness of the proposed intelligent approach, including Support Vector Regression (SVR), Decision Tree (DT), Radial Basis Function (RBF), and Fuzzy Inference System (FIS). Experimental data on critical current values of ReBCO tapes subjected to multiple and repetitive overcurrent cycles were employed for this investigation. The results demonstrated that the Mean Relative Error (MRE) of the SVR method is 23%, for the DT model is approximately 0.61%, the MRE of the FIS model is well above 0.06%, and the MRE value for the RBF method is about 1.1×10^{-6}%. Moreover, the proposed AI models offer fast test times, ranging from 1 to 11 ms. These findings highlighted the potential of using AI techniques to enhance the estimation accuracy of the risks associated with overcurrent events.

1. Introduction

To reduce the increase rate of Earth's bulk temperature, many countries, including the United Kingdom (UK), are participating in the decarbonization programs. The energy and transportation sectors are two major industries responsible for high amount of greenhouse gases by combusting fossil fuels in conventional power plants and propulsion systems of transportation units. To reduce the carbon footprint, electrical power generation through renewable energy resources and fusion plants together with electrification of the transportation units are proposed [1]. Here, the main challenge is that conventional electrical devices have high losses, low power densities, high weights, and large sizes that make them too bulky and expensive for energy and transportation sectors. To tackle these issues, High Temperature Superconducting (HTS) materials have been proposed, where they increase the power density of electrical devices and reduce energy losses, while they have an environmentally friendly nature [2,3]. Thus, HTS devices, consisting of Coated Conductors (CCs) based on Rare-earth Barium Copper Oxides (ReBCO), will become promising solutions in electrical power systems and stand-alone electrical grids of ships, trains, and aircraft, in future.

Overcurrent cycling, overheating cycling, and mechanical overload cycling are factors that reduce the expected life of HTS devices by reducing the overall critical current of CCs. Many efforts have been made to characterize the critical current of HTS tapes, under different electrical [4–7], thermal [8], and mechanical overloads [9–12]. In this regard, overcurrent cycling is referred to 5x-20x current increase of the HTS device that lasts for 15 cycles or more [13,14]. Although Overcurrent incidents are inevitable, they are highly likely to significantly diminish the Average Critical Current (ACC) of ReBCO tapes/wires, thereby increasing losses, generating local heating, causing hotspots, and essentially impacting the Remaining Useful Life (RUL) of HTS devices. Indeed, by the occurrence of overcurrent events, the ACC of a

* Corresponding author.
E-mail address: mohammad.yazdani-asrami@glasgow.ac.uk (M. Yazdani-Asrami).

https://doi.org/10.1016/j.mtphys.2024.101365
Received 15 December 2023; Received in revised form 12 January 2024; Accepted 7 February 2024
Available online 15 February 2024

superconductor starts to reduce due to thermal stresses on the superconducting layer. Finally, the CC would be damaged after multiple times of overcurrent events and ACC would be reduced so that the safety and stability of HTS devices are jeopardized. This phenomenon arises from the reduction of ACC within an HTS tape, which can trigger premature quenching, and ultimately result in HTS device failure.

To avoid any failures and malfunctions in HTS devices, studying the Critical Current Degradation Rate (CCDR) after overcurrent is critically important. It is pivotal to estimate the remaining number of overcurrent cycles that an HTS device can handle without ACC degradation in a safe range where the operation of the device is not jeopardized. In this manner, important parameters of CCDR testing are the magnitude and frequency of overcurrent, operational temperature of HTS tape, initial critical current of the HTS tape, and geometrical/physical properties of HTS tapes. In Ref. [15], an experimental effort has been conducted on the overcurrent characteristic of nine ReBCO samples. The imposed overcurrent is a 50 Hz AC with three different amplitudes which are namely, 200 A, 300 A, and 400 A with different times ranging from 100 ms to 400 ms. Another experimental study has been performed by Ref. [16] to investigate the impact of tape structure on the CCDR after overcurrent. The thickness of the stabilizer layer was changed while the approximate amplitude of overcurrent is 900 A which lasts for 80 ms. In Ref. [17], a 3D Finite Element Model (FEM) is developed to study the thermal impact of overcurrent on CCDR. The amplitude of overcurrent in this varied from 250 A to 340 A while the initial value of critical current was about 120 A. A numerical model is proposed in Ref. [18], to investigate the CCDR caused by overcurrent and mechanical overloading. The imposed overcurrent varies from 220 A to 240 A which is injected into the tapes in the form of pulsed current. An experimentally validated model is proposed in Ref. [19] that investigates the impact of lightning overcurrent on the CCDR of the ReBCO tapes. The amplitude of the overcurrent is 30 kA while the duration is 0.4 μs. Two data-driven models, the Life Prediction Model (LPM) and the Similarity-Based Method (SBM), are used in Ref. [7], to estimate the CCDR in ReBCO tapes, caused by overcurrent. In this regard, initially, experimental tests on 4.4 mm wide, 200 μm thick HTS have been conducted [7]. The samples of this reference are 20 copper-encapsulated second-generation YBCO tapes. Different samples were cut from the same reel of YBCO tape sequentially to make sure that the CCDR processes of these samples, under overcurrent, are as similar as possible. However, YBCO tapes have cracks through their length at the initial state due to mechanical cutting. That results in different CCDR characteristics in different samples. Another difference between different samples is that the manufacturing process makes it impossible for the thickness of the superconducting layer to be completely uniform in all areas of the reel [7]. Then, the data are fed into the models to characterize the CCDR of different samples. Here, despite the alignment of estimated values with measured data trends, the Mean Relative Error (MRE) exceeds 8% at minimum. It should be improved to be able to satisfy the requirements of engineers and manufacturers during the design of HTS devices. Besides, mathematical data-driven models consider the trend of data and fit themselves with this trend. It demands a novel method that not only fits with the trend of data but also analyses the data individually to increase the accuracy and adaptability of the CCDR estimation. In other terms, unlike the fitting methods that just consider the trend of data, models are needed to not only consider the trend in data but also consider the changes of each data individually to increase the accuracy and adaptability. Efforts should be taken to address the gap in accurate and adaptable estimation methods of CCDR that simultaneously consider the trend of data and the data individuality.

In this paper, novel approaches based on Artificial intelligence (AI) techniques are proposed for estimating the CCDR during multiple overcurrent cycles. For this purpose, support vector machines, decision trees, fuzzy interference systems, and radial basis networks have been used. The data used for these methods are experimental data that have been reported in the literature. Results have shown that the proposed AI-based methods have a mean relative error of lower than 1%, for the optimum hyperparameters. For the selection of the hyperparameters, a sensitivity analysis has been conducted to ensure that the reported hyperparameters result in the highest accuracy of the proposed models. It should be noted that hyperparameters are parameters related to the structure of the AI-based models that are set before the learning process begins. Hyperparameters can be tuned and would directly affect how well an AI-based model trains and learns the trend of the data.

2. Intelligent modelling methodology

To predict the CCDR of the HTS CCs, intelligent methods are proper choices for predictive and real-time estimation in electric transportation units. This is critically important to be done by accurate and fast techniques to increase the safety and reliability of the electric system. For such purposes, accuracy and speed play important roles in offering highly accurate, fast response time, and adaptability for estimation of the critical current reduction rate, after the fault is cleared in the power system [20–24].

2.1. Decision tree model

Decision Tree (DT) is one of the machine learning methods that is used for classification, regression, and prediction of complex systems characterisation [25,26]. It is a visual representation of a series of decisions made based on features that help predict the target variable's outcome. DT has a hierarchical-like structure that is initiated from a root node starts branching out towards the internal nodes and ends up with a leaf node, just like a tree. In this context, the root node is the raw data set before any decision-making happens. The internal node is a point where the decision-making procedure happens based on the features of the data. A leaf node is also defined as the final output of the DT model that could be used/updated for data estimation/prediction. The goal of DT-based models is to form splits that end up with homogenous data subsets. In other words, at each decision point, an "if' condition is established, and depending on whether the answer is true or false, another condition is introduced at the subsequent level of the DT to refine the set of common features. This process continues until a final decision, pinpointing a specific category, is reached where the data are completely pure, the discussion about the meaning of data im/purity will be conducted later in this section. In general, this method starts with choosing the features and thresholds that could separate data, so that they are in the best split. The best split is achieved by minimization of error criteria, such as mean squared error. As stated before, the DT starts with a root node and then, at the first stage, the whole dataset is divided into two subclasses, based on features. Again, based on the features and homogeneity in each of the subsets, the previous splitting procedure is repeated to further the separation of subclasses and increase the homogeneity of the resulting subsets. This continues until the stoppage criteria are met which could be the maximum number of levels. At this stage, which is known as the leaf node, no further splitting happens and the highest possible homogeneity for data is achieved. Finally, each branch of the level has its properties and features, and new test data could be injected for test/prediction purposes. More information about this method can be found in Refs. [27–30].

A schematic of a DT, in Fig. 1, is made to illustrate how a Correct Decision (CD) is chosen among all other possible decisions. DT uses a tree-like behaviour to calculate the possible consequences, probable chance of a specific event, etc. In DT, after preprocessing of data, and based on inputs fed into the DT model, a decision is made at the first level to separate the data into homogenous subsets concerning target values. Then, in the next level, subsets are re-split into more subsets based on the input data, in each decision-making level. This procedure goes on until stoppage criteria are met which could be a maximum number of levels or maximum depth.

Splitting measures are the most important steps toward a high-

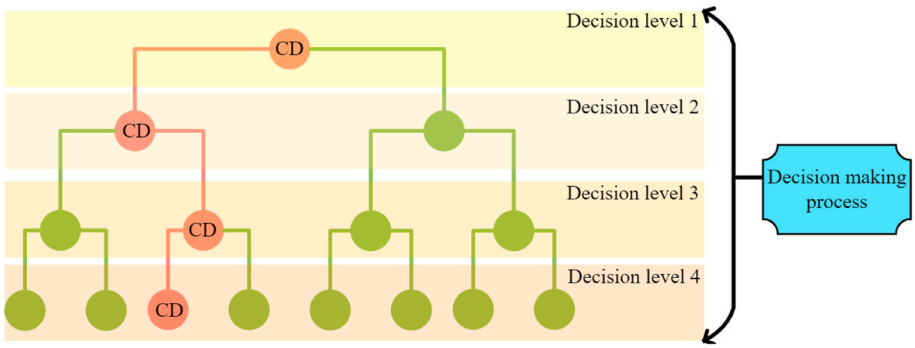

Fig. 1. A schematic of the DT method.

accuracy estimation/classification based on input data. Splitting is conducted through a decision-making process based on a set of hierarchical if-else conditions. DT starts with an original set (S) as a root node which is the whole data set at the beginning. In each iteration, it calculates the Entropy (E), Information Gain (IG), and Gini Index (GI) for each dataset where in each iteration, it selects the data with the highest E and lowest IG. It should be noted that iteration is a fundamental process that is used in the learning stage of AI-based models. It involves the repetitive execution of specific procedures to improve a system's performance and accuracy. In this context, E is defined as the amount of information required to accurately describe data characteristics. Thus, the homogeneity of data that means that all elements are similar, E is 0, and the data is pure. Else if data is inhomogeneous E is higher than 0 and moves towards 1, in other terms data is impure. Therefore, E is one of the measures used for the classification of data based on their purity, as it is calculated in equations (1) and (2). Then, there is another measure for data impurity which is known as GI. Same as entropy, GI has a value between 0 and 1, where 0 means pure samples while 1 shows the total inequality among the data elements. GI is also calculated in equation (3) [31]. Finally, there is IG which is defined as a measure that helps to decide the most informative feature to split the data at each node of the tree. The aim of this is to select the feature that separates the data into different classes or reduces the E, with the best performance. IG is determined in equation (4) [31]. Now let's see how these measures help the decision-making process.

The role of IG in the decision-making process is to quantify the impact of a designated feature for the reduction of E in the data set. In other words, by determining the IG, E difference before and after the split is determined. Therefore, a higher IG results in more pure/homogenous data after the split, so the decision-making should be conducted towards the highest value for IG. On the other hand, the role of GI is to measure the quality of the "split" as a procedure not the quality/purity of data after the split. In this context, for decision-making, the lower value of GI has the higher priority. Finally, there is E which is used to calculate the homogeneity of a data set in subsets created by different splits. As stated, DT is more of an "if-else" procedure that is updated based on the updated information of data [31]. In this regard, "attributes" is defined as a piece of information that is used to determine the properties of a field or tag in a database.

$$E(s) = \sum_{i=1}^{c} -p_i \log_2 p_i \tag{1}$$

$$E(T,X) = \sum_{c \in X} P(c)E(c) \tag{2}$$

$$GI = 1 - \sum_{i=1}^{c} (p_i)^2 \tag{3}$$

$$IG(T,X) = E(T) - E(T,X) \tag{4}$$

where, p_i is the probability of an event i of state S or percentage of class i in a node of state S, T is the current state, and X selected attribute.

2.2. Fuzzy interference system model

Fuzzy logic, rooted in human logic and the consideration of partial truths, is the main idea behind the Fuzzy Inference Systems (FIS) [32]. FIS employs a set of fuzzy conditional rules (if-then conditions) to recognize the characteristics of a phenomenon. When designing a fuzzy system, the extraction of effective rules and the selection of efficient membership functions are of paramount importance. It should be mentioned that in fuzzy logic, the concept of membership is defined as the degree or extent to which data belongs to a specific set or group. Unlike classical logic, where an element either completely belongs or does not belong to a set or group. This is because errors in these choices can significantly impact system performance. In simpler cases, rule and function selection is often done through trial and error. However, for complex problems, this process becomes very challenging and time-consuming when implemented on regular personal computers [33]. The operation basic of FIS-based models is fuzzy sets, where each data point has a degree of membership functions. Here, the degree of membership function shows the degree to which an input value belongs to a particular cluster. In other words, it maps each input to a cluster by considering its membership function value. For instance, consider that three clusters exist, cluster A, cluster B, and cluster C. For each cluster, a data point has membership function values of 0.2, 0.8, and 0.0, respectively. This means that the considered data point probably belongs to cluster A, otherwise it belongs to cluster B, and is never part of cluster C. The degree of membership function is a number varying from 0 to 1. Equation (5) shows the membership function $\mu_B(x)$ of dataset B for input data of X [34]:

$$B\{x, \mu_B(x) \mid x \in X\} \tag{5}$$

Usually, triangular, trapezoidal, Gaussian and generalized bell-shaped membership functions are considered for FIS modelling. Fig. 2 shows these membership functions plotted versus X, where X is the input of the Fuzzy interference model.

Fuzzy logic starts with an input, converts it into a fuzzy representation, and subsequently directs it to a FIS. Within the FIS, it associates fuzzy input categories with fuzzy output categories by integrating rules from the fuzzy rule base, ultimately yielding a clear-cut output through defuzzification. Numerous inference systems are at one's disposal; however, for crucial current parameterization tasks, the Sugeno inference system is favoured due to its high computational efficiency. Equation (6) representing a Sugeno inference rule is presented below [34]:

$$If\ Input\ 1 = x\ \ and\ \ Input\ 2 = y, then\ \ Output\ is\ z = \alpha x + \beta y + \kappa \tag{6}$$

It should be noted that "z" is the output of the fuzzified stage of the FIS-based model which is a combination of different inputs x and y.

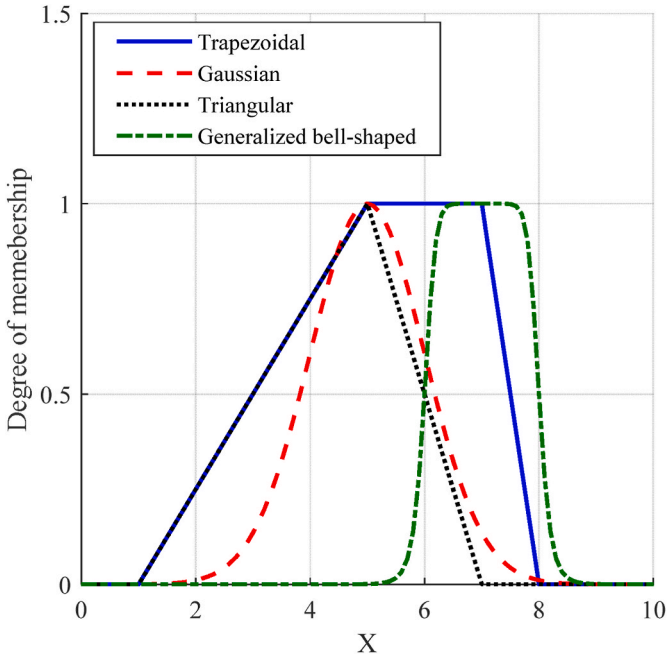

Fig. 2. Membership functions of the FIS-based estimation techniques.

In a FIS, the logical operator of "*and* " is to be presented by equation (7) [35].

$$\mathrm{X\ AND\ Y} = \min(X, Y) \tag{7}$$

Also, in a FIS, the logical operator of "*or* " is to be presented by equation (8) [35]:

$$\mathrm{X\ OR\ Y} = \max(X, Y) \tag{8}$$

In equation (7), the "AND" involves considering the minimum of the membership values of two or more fuzzy sets or propositions to determine their intersection. For instance, let's assume that two fuzzy sets are available: "tall" and "young." If one aims to find the intersection of "tall" AND "young" of a person, the minimum of the membership values of "tall" and "young" should be considered to determine their combined membership value. This represents how much a person simultaneously belongs to both the "tall" set and the "young" set. In equation (8), the "OR" operation consists of considering the maximum of the membership values for two or more fuzzy sets to determine their union. Again, considering the same "tall" and "young" concept, if one aims to find the union of "tall" OR "young", the maximum of the membership values of "tall" and "young" must be considered to determine their combined membership value. This represents how much a person belongs to either the "tall" set the "young" set, or both.

To be used in a fuzzy logic model, the data must fall within one of the membership functions. These membership functions represent clusters. Each cluster signifies the category to which the input data belongs, and the FIS generates an output accordingly. Essentially, clustering involves the grouping of similar data [34]. The clustering techniques employed in this context include grid partition clustering, fuzzy C-means clustering and the subtractive clustering method (SCM) which are the most common clustering techniques in literature and are formulated in Ref. [36]. Fig. 3 shows an overview of an FIS considering different parts. More information regarding the fuzzy logic method can be found in Refs. [37–40].

In general, estimating the outputs by using inputs through FIS could be concluded as the following steps:

- Fuzzification: changing the crisp/numerical input data into fuzzy sets using linguistic variables and membership functions.
- Fuzzy rule designation: considering fuzzy rule sets so that they relate input variables to output variables. These rules typically follow an "IF-THEN" structure and capture expert knowledge or system behaviour.
- Fuzzy inference: This step includes the application of fuzzy logic operations such as fuzzy "OR" and fuzzy "AND" by using the defined rules and the membership values of input variables to determine the degree of support of each rule.
- Aggregation: Combine the activated rules using methods like max, min, or weighted average to obtain an aggregated fuzzy output.
- Defuzzification: Convert the aggregated fuzzy output into a crisp value or decision.

2.3. Support vector regressor model

Support vectors are a well-known family of machine learning algorithms, which is used for both classification (Support Vector Machine, SVM) and regression (Support Vector Regression, SVR) problems. The generalization ability to handle many types of datasets (even the highly non-linear problems) with high accuracy makes it a popular method among researchers. To reach this, the support vector aims to find a hyperplane in the higher dimensional transformed data that has a maximum margin and a minimum error. Ideally, the margin is defined as the region near the hyperplane where there should not be any data points. Therefore, a tolerance (ϵ) value for error must be considered to leave these points remaining in the margin which are known as support vectors. Support vectors have a direct influence on the orientation and position of the hyperplane and the boundaries. A general presentation of SVR methods is shown in Fig. 4. More details and considerations about SVR can be found in Refs. [41–43].

The non-linear data can be represented by a fitting equation which is formulated by SVR as equation (9) [44]:

$$f(x) = w^{v}\varphi(\mathrm{x}) + \mathrm{b} \tag{9}$$

where, w is the weight fand actor, φ is the function that SVR uses to generate data in high-dimensional space using the input data to reach a

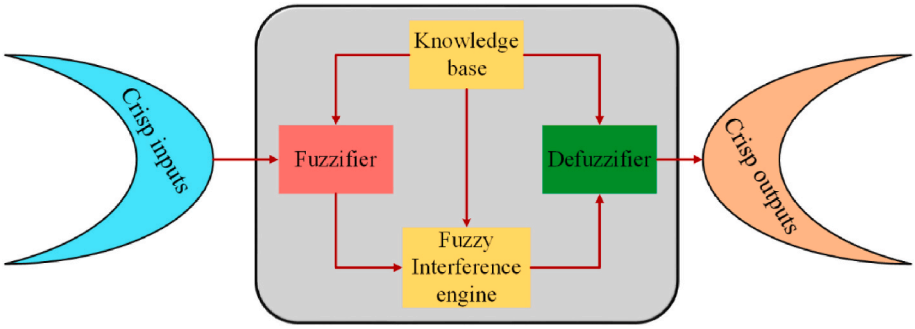

Fig. 3. A schematic of an FIS-based model.

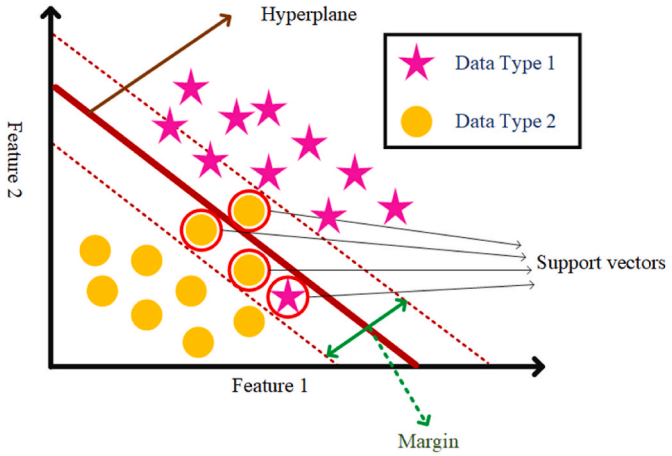

Fig. 4. A general presentation of the SVR method, where X-axis refers to the input value of each data point while Y refers to the output value specified to each data point.

better relation between variables and therefore, reduce the error. Also, the SVR algorithm tries to use the training dataset and minimize the following equation to find the best model with the lowest inaccuracies, as shown in equations (10) and (11) [45]:

$$Minimize\ equation: \left[\frac{||w||^2}{2} + C\left(v\epsilon + \frac{1}{M}\sum_{i=1}^{M}(\zeta_i, \zeta_i^*)\right)\right] \tag{10}$$

$$subject\ to \begin{cases} f(x_i) - s_i \le \epsilon + \zeta_i^*, i = 1, 2, 3, \ldots \\ s_i - f(x_i) \le \epsilon + \zeta_i, i = 1, 2, 3, \ldots \\ \zeta_i, \zeta_i^* \ge 0, i = 1, 2, 3, \ldots \\ \epsilon \ge 0, i = 1, 2, 3, \ldots \end{cases} \tag{11}$$

where, $\frac{||w||^2}{2}$ is the regularization factor, C is cost function for model's smoothness balancing and ϵ is loss function, v is a controller between 0 and 1 to control the number of support vectors, ζ_i, ζ_i^* are non-negative slack parameters, and M is the number of observations of the training dataset [45].

In this method, the kernel function plays a vital role in Support Vector Regression (SVR). It enables SVR to handle non-linear relationships by changing the data into a more complex space, making it possible for a linear model to grasp intricate patterns. By considering $k(x_i, x_i) = \varphi(x)\varphi(x)$ as kernel function, equation (9) can be rewritten as equation (12):

$$f(x) = \sum_{j=1}^{M}(\zeta - \zeta_i^*)k(x_i, x_i) + b \tag{12}$$

It should be mentioned that the kernel function in the SVR algorithm is used for implicitly mapping the input data points into a higher-dimensional feature space. By doing this, the SVR algorithm can find a linear regression model that separates the data points with a maximal margin while minimizing prediction error tolerance.

2.4. Radial basis network model

Radial basis function neural network (RBFNN) is a type of feed-forward neural network (FFNN) which is used for regression problems. The most distinguishing difference between RBFNN and FFNN is their universal approximation and fast training speed. A typical RBFNN has three main layers including an input layer with the number of neurons equal to the number of input variables, a hidden layer with enough neurons and weight and bias factors to make a relation between the variables, and finally, an output layer to predict the target variables.

In comparison, RBFNN uses a radial basis mathematical function in the hidden layer. Each RBF in the hidden layer calculates its activation by considering the distance between the input data and a specific centre point. Frequently, the radial basis function (RBF) has a form like the one, described in equation (13) [46]:

$$\varphi(r) = \exp\left(-\frac{r^2}{2\sigma^2}\right) \tag{13}$$

In this context, the centre point represents the prototypes or centroids in the input space around which the radial basis functions are cantered. Each centre point corresponds to a prototype or representative point in the input space.

Where r represents the distance of predicted data and the cluster's centre [47]. There are some ways to evaluate this distance. The method that is very common and has been used in this paper is Euclidean distance which r can be evaluated for jth neuron in the hidden layer using equation (14) [46]:

$$the\ \mathrm{r_j} = \sqrt{\sum_{i=1}^{\mathrm{n}}\left(\mathrm{x_i} - \mathrm{w_{ij}}\right)^2} \tag{14}$$

In this equation, x is the input vector and w is network's centre vector. So, by a combination of these two equations, the final output of each neuron in the hidden layer can be calculated by using equation (15) [48]:

$$sigmas\varphi(r) = \exp\left(-\frac{\left|\sum_{i=1}^{n}\left(x_i - w_{ij}\right)^2\right|}{2\sigma^2}\right) \tag{15}$$

By having the final output value of each neuron, RBFNN in each epoch/iteration aims to minimize the objective function shown in equation (16) [49]:

$$E = \frac{1}{N}\sum_{i=1}^{N}\left\|y_i - W^T\varphi(r)\right\|^2 \tag{16}$$

where, y_i is the target value during the regression and is the weight that should be updated in each epoch to increase the accuracy of model. To update the weights in each iteration, a least squares method is used, as presented in equation (17) [49]:

$$W = \left(\Phi\Phi^T\right)^{-1}\Phi Y^T \tag{17}$$

where, Φ is the vector of the outputs and Y is the vector of target values. Indeed, it should be mentioned that epochs represent full passes through the entire training dataset, and iterations represent individual updates based on a batch of data within each epoch. Fig. 5 shows a RBFNN that consist of two inputs (X1 and X2), output layer, and two hidden layers.

2.5. Performance indices

An AI-based model needs to be evaluated by some indices during its training to ensure accuracy. These indices can help us to compare the accuracy of different sets in the sensitivity analysis. The indices that have been used in this paper are the common indices in the field of AI including Root-Mean-Square Error (RMSE), Pearson coefficient (R^2 - to show the goodness of a fit), Mean Relative Error (MRE), and Mean Accuracy (MAC). These indices are shown in equations (18)–(21) [20,50,51]:

$$RMSE = \sqrt{\sum_{k=1}^{n_s}\frac{(d_k - y_k)^2}{n_s}} \tag{18}$$

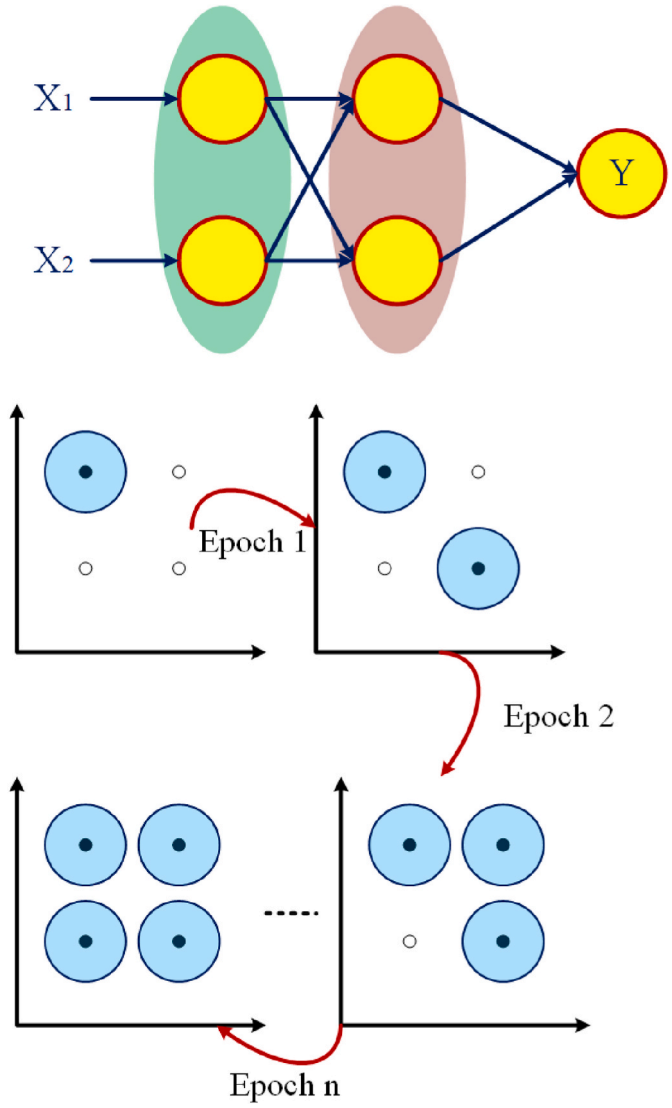

Fig. 5. A general overview on RBFNN.

$$R^2 = \frac{\sum_{k=1}^{n_s}(d_k - \overline{d})(y_k - \overline{y})}{\sqrt{\sum_{k=1}^{n_s}(d_k - \overline{d})^2 \sum_{k=1}^{n_s}(y_k - \overline{y})^2}} \quad (19)$$

$$Mean\ Relative\ Error\ (MRE) = \frac{(d_k - y_k)}{y_k} * 100 \quad (20)$$

$$Mean\ Accuracy\ (MAC) = 1 - \ Mean\ Relative\ Error\ (MRE) \quad (21)$$

3. Results and discussion

This section presents information and properties of the samples, followed by a sensitivity analysis on the hyperparameters of AI-based models. The optimal structure of each AI model is compared, and their accuracy is evaluated against existing data-driven models from the literature, demonstrating superior performance of the proposed method in this study.

3.1. Specification of the HTS tape and overcurrent testing flowchart

The electrical and geometrical ReBCO tape is presented in Table 1, based on the experiments conducted in Ref. [7]. Seven copper encapsulated second-generation YBCO tape samples are cut from the tape of

Table 1
The geometrical and electrical parameters of the studied ReBCO tape [7].

Parameter	Value	Unit
HTS tape width	4	mm
ReBCO layer width	1	μm
Average critical current	100–110	A
Operational temperature	77	K
Copper stabilizer thickness	2 × 50	μm
Hastelloy substrate thickness	70	μm
Silver shield thickness	2	μm
Buffer layer thickness	0.2	μm

Table 1. These samples were obtained by sequentially cutting from the same YBCO tape reel to maintain consistency in their CCDR processes when subjected to overcurrent. However, at the initial stage, the YBCO tapes exhibit cracks along their length due to mechanical cutting, leading to varied CCDR characteristics among the samples. Additionally, the manufacturing process prevents the superconducting layer's thickness from being uniformly consistent across all parts of the reel.

Fig. 6 shows the distribution of CCDR data of different samples after being experimentally tested under different overcurrent cycles, conducted by Ref. [52]. Based on this reference, the test procedure for gaining the experimental results is as follows and shown in Fig. 7 where it also shows the test circuit of the experimental critical current acquisition used by Ref. [52]:

- After three times measuring the critical current of the CC, the mean value of three tests is considered as the initial value of critical current.
- The next step would be conducting the overcurrent test. Here the overcurrent waveform is a 50 Hz, 480 A, and with a duration of 0.44 s. This means that the imposed overcurrent approximately 5 times higher than critical current of samples [52].
- After each three/two times repetition of the overcurrent test, the critical current of the CC is measured, and reported.
- The final two steps are repeated until the ACC of the CCs reduces to be less than 3% of the initial values.

Each of seven samples were tested for more than 10 times until finally, 3% threshold of CCDR was pass. Under each test, different overcurrent cycles have been applied to each sample. This resulted in

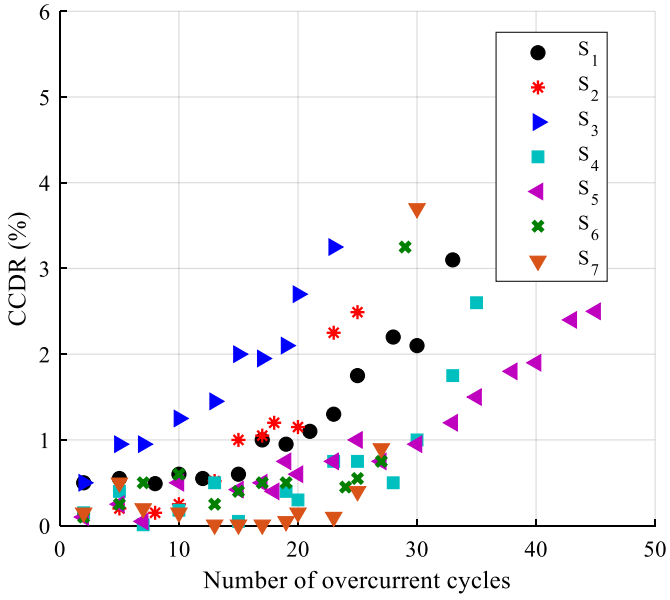

Fig. 6. Experimental data of different samples undergone through different overcurrent cycle test.

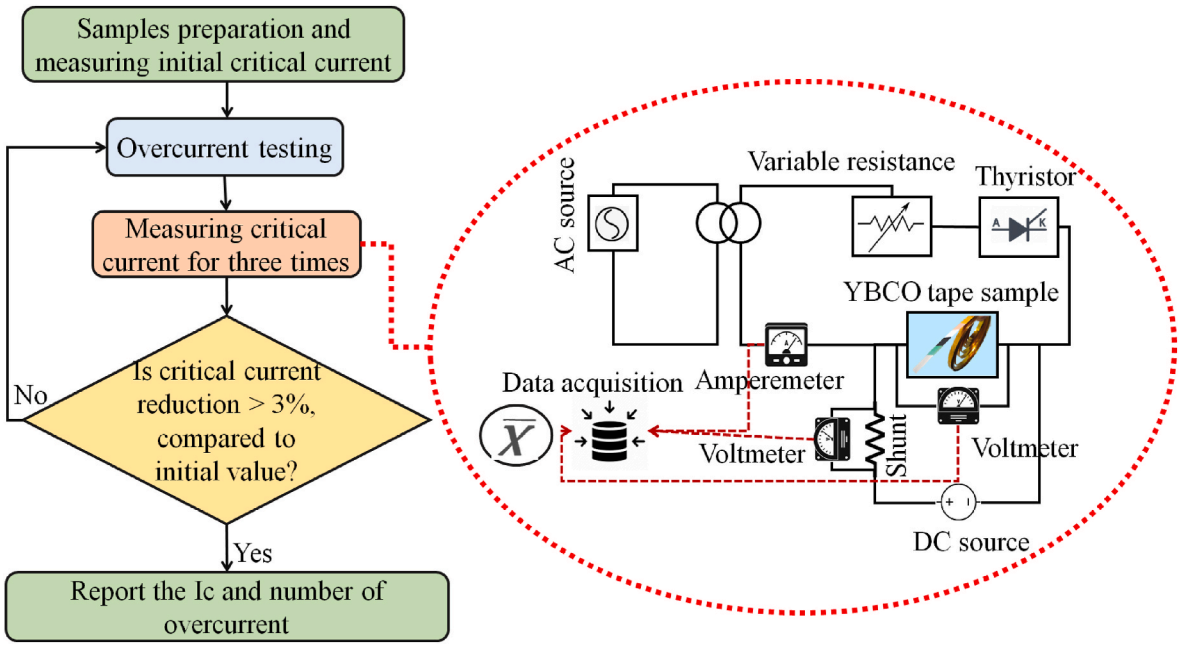

Fig. 7. Experimental test procedure of the ReBCO tapes samples, data acquisition and experimental test set up used in [52].

more than 70 data points to be used for AI-based model. By having these data, the next step is the implementation of AI-based models. This is done firstly through an investigation for selection of the hyper-parameters for each model. In this regard, the inputs are the number of overcurrent cycles and sample number while the output is the CCDR in percentage. It should be mentioned that the term "samples" is referred to the different pieces of the same YBCO tape presented in Table 1. Since the critical current of YBCO tapes has variative characteristics through the length of the tape, the different pieces of the same HTS tape, would react differently under overcurrent events. As a result of this, one YBCO tape was used here for CCDR analysis in this paper, as well as the reference paper.

3.2. Sensitivity analysis on hyperparameters of AI-based models

Sensitivity analysis is a technique that is used to study how changes in hyperparameters affect the estimated outputs of an AI-based model. The main goal of such a study is to understand the relationship between the different hyperparameters of an AI technique and the accuracy of output estimation.

3.2.1. Hyperparameters tuning for DT model

In this section, the impact of DT hyperparameters on the final accuracy of critical current degradation is discussed. The number of trees is changed from just 1 to 30, as shown in Table 2 and Table 3, where their impact is analysed on the accuracy of the estimation metrics and training/test time. By considering the number of trees as 1, the minimum MRE is 3% and maximum is 28% while the simulation time is about 1.65 ms. After increasing the number of trees to 5, the MRE is significantly reduced. In this case the maximum MRE value is reduced well above 58% compared with the first case with 1 tree. Although the MRE is reduced significantly, it still has high value in some samples which should be reduced further. To achieve this, number of trees have been increased further to 10, where maximum value of MRE is reduced well above 47% while the minimum value of MRE is just reduced to 7%, compared with the situation where number of trees was 5. Also, the test time of the model where number of trees is 10, increases approximately 75% compared to the model with 5 trees. On the other hand, increasing the number of trees from 10 to 15, results in 50% reduction of maximum MRE, while the test time is increased well above 7% and the train time approximately 18% increases. If another time, the number of trees increases from 15 to 20, the maximum MRE is again 70% reduced while test time is increased by 33% and the train time is 10% more at this stage. Finally, by the increase of the trees number from 20 to 30, maximum MRE would be less than 1%. Whilst the train time approaches to near 1 s which is quite long. By observing the whole trend in the results of Tables 2 and 3, the MRE of the DT-based model is reduced by increasing the number of trees while the computational times are significantly increased. Also, by considering the S_1 sample, it would be observed that MRE is well above 8% when decision tree is 1. By increasing the tree number to 5, the MRE is 58% reduced while test time is increased approximately 100% increased. Then, by further increasing the tree number to 10, the MRE of this sample 55% reduces and the test time faces 75% increase, and the train time faces 71% increase. By doing this analysis, it is obvious that by increase of the trees number, not only the maximum MRE is reduced but also MRE of each individual sample reduces. This is an approvement on the pre-discussed concept of AI-based methods that unlike fitting methods, AI cope itself with respect to data trend as well as the data individuality.

Table 2
Mean relative error, MRE (%) of DT model.

Number of trees	1	5	10	15	20	30
Samples						
S_1	8.62	3.65	1.61	0.83	0.54	0.02
S_2	14.78	4.98	1.69	1.31	0.32	0.23
S_3	10.57	4.21	2.67	1.28	0.59	0.49
S_4	3.84	1.31	1.2	0.49	0.24	0.07
S_5	21.52	7.50	4.60	3.05	1.43	0.82
S_6	28.39	11.59	5.99	3.52	1.09	0.63
S_7	14.15	16.08	6.4	3.21	0.32	0.26

Table 3
Test and train times (ms) of DT model for all ReBCO samples.

Number of trees	1	5	10	15	20	30
Test Time (ms)	1.65	3.24	5.66	6.01	8.09	10.29
Train Time (ms)	136	268	457	644	712	976

3.2.2. Hyperparameters tuning for FIS models

Table 4 and Table 5 tabulate the MRE values in estimation of CCDR after overcurrent with respect to grid partition clustering method by FIS technique. A number of clusters have been changed ranging from 2 to 11 to study their impact on the final accuracy of the estimation. When, number of membership functions is 2, the maximum MRE value, that happens for sample 7, is 1620% and the test/train time is 1.12/113 ms. Then, by increasing the number of membership functions from 2 to 3, the maximum MRE 80% reduces while the test and train times are 34% and 19% increased. Although the maximum MRE was reduced significantly, it has still an unacceptable value of 300%. Thus, further increase in the number of memberships functions is necessary. Even for 5 membership function, still maximum MRE is higher than 100% which is not practical. Surprisingly, after increase of membership functions number to 11, the maximum MRE value remains barely constant while the train and tests times are increasing. In conclusion, it should be noted that the current grid partitioning method is not applicable for gaining a high estimation accuracy by FIS-based regression.

To study the impact of different clustering method on the accuracy of the FIS model, another clustering method is used, known as the C-means clustering method. Table 6 and Table 7 show the changes of MRE value regarding the variations of cluster numbers in C-means method. Firstly, 2 clusters are considered that results in maximum MRE of 1450% and the train/test time of 101/1.15 ms. Then, by increasing the number of clusters to 3, the maximum MRE is approximately 10x reduced while the train/test time is 41%/44% increased. The maximum MRE reduced further by increasing the number of clusters from 3 to 5 where it faces a 33%. In this case, the test and train times faces 24% and 11%, respectively. Thus, it should be stated that by increasing the number of clusters the accuracy of the model as well as the train and test times are increased. Finally, it is observable that under 11 clusters, the maximum MRE is reduced significantly to 12% while test and trains times increase significantly, more than 90%. It should be stated that, although for 11 clusters most of the MRE values are lower than 2%, the maximum MRE is still high for exact CCDR estimation. Thus, it could be stated that this type of clustering is unable to predict the CCDR in an accurate manner.

Another clustering method, known as SCM is used to study the feasibility of FIS techniques in accurately estimating the CCDR of different samples. In this clustering method, the radius of clusters plays an important role. Thus, changes of cluster radius and their impact of accuracy is studied with respect to the results presented in Table 8 and Table 9. By considering the cluster radius equal to 0.6, the maximum MRE of the model is above 3610% with the train/test time of 103 and 1.19 ms. To reduce the maximum MRE, the cluster radius is selected to be 04 that results in significant reduction of maximum MRE to 190%. Although this value is still high, the significant reduction of maximum MRE, shows that reduction of clustering radius could end up with accuracy increase of the model. Based on this, radius is reduced to 0.2 while the maximum MRE face a huge reduction approximately equal to 84%. In this state, the train and test times of the model are about 32% increased. The next step to reduce the cluster radius from 0.2 to 0.01 to observe the impact of small cluster radius on the accuracy of the model. By doing this, surprisingly, the maximum MRE of the model is reduced to lower than 0.2% with train and test times of 638 ms and 9.95 ms, respectively. The reason of such significant reduction is that by considering the clustering radius equal to 0.01, the number of clusters (or cluster centres) are increased that could increase the accuracy of the model, in this case. By observing these values of SCM clustering, it should be stated that, among the FIS-based models, the SCM-based FIS has the best performance and selected to be compared with other methods.

Table 4
Mean relative error, MRE (%) of FIS model with grid partition clustering method.

Membership function number	2	3	5	7	9	11
Samples						
S_1	17.58	7.43	6.62	3.98	2.78	0.075
S_2	22.22	11.10	10.55	2.39	0.03	0.004
S_3	7.49	6.44	4.19	0.24	0.0059	0.001
S_4	365.00	208.09	137.57	18.94	0.023	0.011
S_5	28.36	33.88	27.82	29.59	26.55	24.14
S_6	199.84	31.52	7.82	0.13	0.0043	1.6e-4
S_7	1620.1	325.92	76.84	34.02	0.1603	0.02

Table 5
Test and train times (ms) of FIS model with grid partition clustering method, for all ReBCO samples.

Membership function number	2	3	5	7	9	11
Test Time (ms)	1.12	1.51	1.88	3.01	3.09	4.85
Train Time (ms)	113	134	99	262	318	467

Table 6
Mean relative error, MRE (%) of FIS model with Fuzzy C-means clustering method.

Cluster number	2	3	5	7	9	11
Samples						
S_1	30.36	7.43	4.93	3.82	1.07	0.19
S_2	26.07	14.24	3.99	0.26	0.01	3e-5
S_3	6.89	6.48	1.91	0.06	0.004	1e-6
S_4	378.17	238.17	159.59	25.39	5.36	0.78
S_5	30.15	32.83	30.52	26.02	17.35	12.14
S_6	229.29	101.27	8.99	4.22	0.45	0.003
S_7	1450.2	149.58	37.81	14.93	7.67	1.21

Table 7
Test and train times (ms) of FIS model with Fuzzy C-means clustering method, for all ReBCO samples.

Cluster number	2	3	5	7	9	11
Test Time (ms)	1.15	1.66	1.85	2.55	3.11	6.14
Train Time (ms)	101	143	178	239	355	431

Table 8
Mean relative error, MRE (%) of FIS model with Sub-clustering method.

Cluster radius	0.6	0.4	0.2	0.01
S_1	20.11	15.68	6.67	0.0012
S_2	12.51	9.25	9.78	0.0353
S_3	6.57	6.06	4.93	8.54e-4
S_4	236.33	190.62	1.24	0.178
S_5	28.42	30.13	29.98	0.127
S_6	155.12	20.07	3.59	4.95e-4
S_7	3160.01	79.72	27.80	0.0829

Table 9
Test and train times of FIS model with Sub-clustering method, for all ReBCO samples.

Cluster radius	0.6	0.4	0.2	0.01
Test Time (ms)	1.19	1.66	2.19	9.95
Train Time (ms)	103	159	211	638

3.2.3. Hyperparameters tuning for SVR model

SVR has two important hyperparameters. In this paper, the impact of training error (C) and non-linearity level of kernel function σ hyperparameters is studied. After performing an optimization on these parameters, the best values have been selected for different samples. The

results are shown in Table 10 for CCDR estimation of different samples. The estimation MRE value with SVR method is 23%–200% which is very high for such purpose. As a result of this, the SVR technique could not be used for this purpose. However, this should be pinpointed that the train time of SVR-based model has the lowest value among all other AI-based methods. Also, the test time of this method in some cases is higher than other methods, such as estimation for sample 3 which has the test time about 11 ms.

3.2.4. Hyperparameters tuning for RBFNN model

The RBFNN has two important hyperparameters, namely, spread of network and number of neurons. Regarding these hyperparameters, Fig. 8 shows the impact of these hyperparameters of MRE for different samples. As it can be observed, by increasing the number of neurons the accuracy of the model increases and increasing the spread of RBF, reduces the error of the model. For S_1, when the spread pf network is about 1 and the number of neurons is 25, the MRE of the model is approximately 25% while by keeping the neurons number constant and increasing the spread of network to any number higher than 5, the MRE will be reduced to less than 1%. However, by increasing the number of neurons while considering the constant value for spread of network, MRE will be reduced to about 10%. This is also the case, for other samples, where increasing the spread of network has more impact on MRE reduction, compared to number of neurons. Thus, it could be stated that the designation of proper value for spread of network plays a more crucial role in MRE reduction of the model, compared to number of neurons value. This can be also approved that in some cases, keeping the spread value of the systems as constant value while increasing the number of neurons does not reduce the MRE of the model and increases it, like S_2. In all samples, for spread value lower than 5, MRE reduces to less than 1% for all samples and all choices of neuron numbers. It should be noted that, the results shown in Fig. 8, are the mean value of 50 iterations.

3.3. Optimized results and analysis

After sensitivity analysis on the impact of hyperparameters on MRE index of different methods and deciding that SVR methods could not be used for CCDR purposes since it has a significant error, this section deals with comparing the estimation results of best structure in each estimation method.

Fig. 9(a) shows the final estimation results by RBFNN method. As can be seen, the resulted curve is in an excellent coordination with experimental results. The resulted curve not only follows the trend of data inside of the fitting zone but also shows an incremental characteristic for the zone without any data. Although there are no data available in this zone, we know that any further overcurrent event, will results in more CCDR. Thus, the predicted trend of data within this zone is expected to be consistently incremental, aligning with the trend visually depicted in Fig. 9(a). Fig. 9(b) illustrates the estimated curve by DT system which is also in an excellent coordination with experimental results. Finally, Fig. 9(c) is related to the results of FIS-based estimation which has also a high level of accuracy while in some points, such as data-points of sample 5, it has lower accuracy comparing two previous methods.

It should be mentioned that there are several advantages of AI-based regressions over conventional fitting methods where regression using AI techniques could outperform traditional fitting methods in certain scenarios such as:

- **Dealing with complexities**: AI-based regression models can handle complex relationships between inputs and the outputs by identification of patterns in the data. So, by having different samples from different HTS tapes with different sublayer structures and critical current, fitting methods such as piecewise linear could not be used. This is because of that more than two or three inputs could be fed into the conventional fitting methods.
- **Nonlinearity**: Traditional fitting methods like linear regression or polynomial regression assume linear relationships between variables. AI-based regression models, such as neural networks, can learn non-linear relationships, making them more adaptable to complex, non-linear data distributions.
- **Scalability**: AI techniques, can handle vast amounts of data more efficiently than some traditional fitting methods. They often scale well with larger datasets, allowing for potentially more robust predictions as the amount of data increases. While the accuracy of the conventional fitting methods reduces by increasing the number of data, since each data could have a specific characteristic.
- **Generalization**: AI models can exhibit better generalization capabilities, meaning they can often perform well on unseen data, known as extrapolation. This is especially true for AI techniques which can generalize across various patterns and trends within the data.
- **Adaptability**: AI-based regression models are often adaptable to various types of data and problems. They can be fine-tuned, retrained, or modified to suit different scenarios, making them versatile compared to some traditional fitting methods that might be more rigid in their application.

Table 11 tabulates the RMSE, R, and Mean Accuracy (MAC) indices of different methods for CCDR estimation to make their comparison more conceivable in terms of numbers. Highest RMSE value of RBFNN method relates to sample number five with a 10x to 100x higher RMSE value comparing to other samples. However, the accuracy of this sample is quite high with a MAC value of 99.999999%. The lowest accuracy in DT model relates to sample number six with RMSE value of 0.04 which is about 1000x higher than worst case in RBFNN. Finally, the MAC value of FIS method for samples four, five, and seven is less than 95% which shows the incapability of this methods in CCDR estimation. Thus, among these methods, the RBFNN technique has the upper hand and privilege to other methods.

The proposed methods in this paper have high value accuracy, and they outperform the techniques exists in literature. Table 12 tabulates the MRE (%) and RMSE (%) values of two methods proposed in literature, known as Life Prediction Model (LPM) and Similarity-Based-Method (SBM) [52] comparing to the MRE values of methods proposed in this paper as well as the three fitting equations. The MRE value of FIS, as the AI-based method with lowest accuracy, is 1300% lower than proposed methods in literature, while it also outperforms the fitting methods with more than ten times lower value. DT method has also high estimation accuracy and low error with R value of 0.9999, MRE of 0.06, and RMSE value of 0.0129. Thus, this method has also a better performance, compared to LPM, SBM, and fitting methods. Finally, there is RBFNN, as the best AI-based model with 1.1×10^{-6} MRE and RMSE near zero. This shows the capability of AI-based methods for CCDR estimation of ReBCO tapes. The MRE value of AI-based models is also extremely lower than the MRE value of three mathematical fitting equations, shown in Table 12. On the other hand, AI-based models have lower MRE values compared to rest of the methods. This approves that just AI-based models consider the individuality of data.

Table 10
Mean relative error, MRE (%), test time (ms) and training time (ms) of SVR method.

Sample	value of training error and the margin (C)	Value of non-linearity level (σ)	MRE (%)	Test time (ms)	Train time (ms)
S_1	10	1	43.12	2.14	18.8
S_2	10	2	59.13	5.11	14.5
S_3	10	1	23.11	10.95	19.5
S_4	40	9	85.33	6.11	10.4
S_5	40	2	121.13	6.55	13.6
S_6	10	2	66.48	6.19	15.2
S_7	50	9	207.74	6.01	19.1

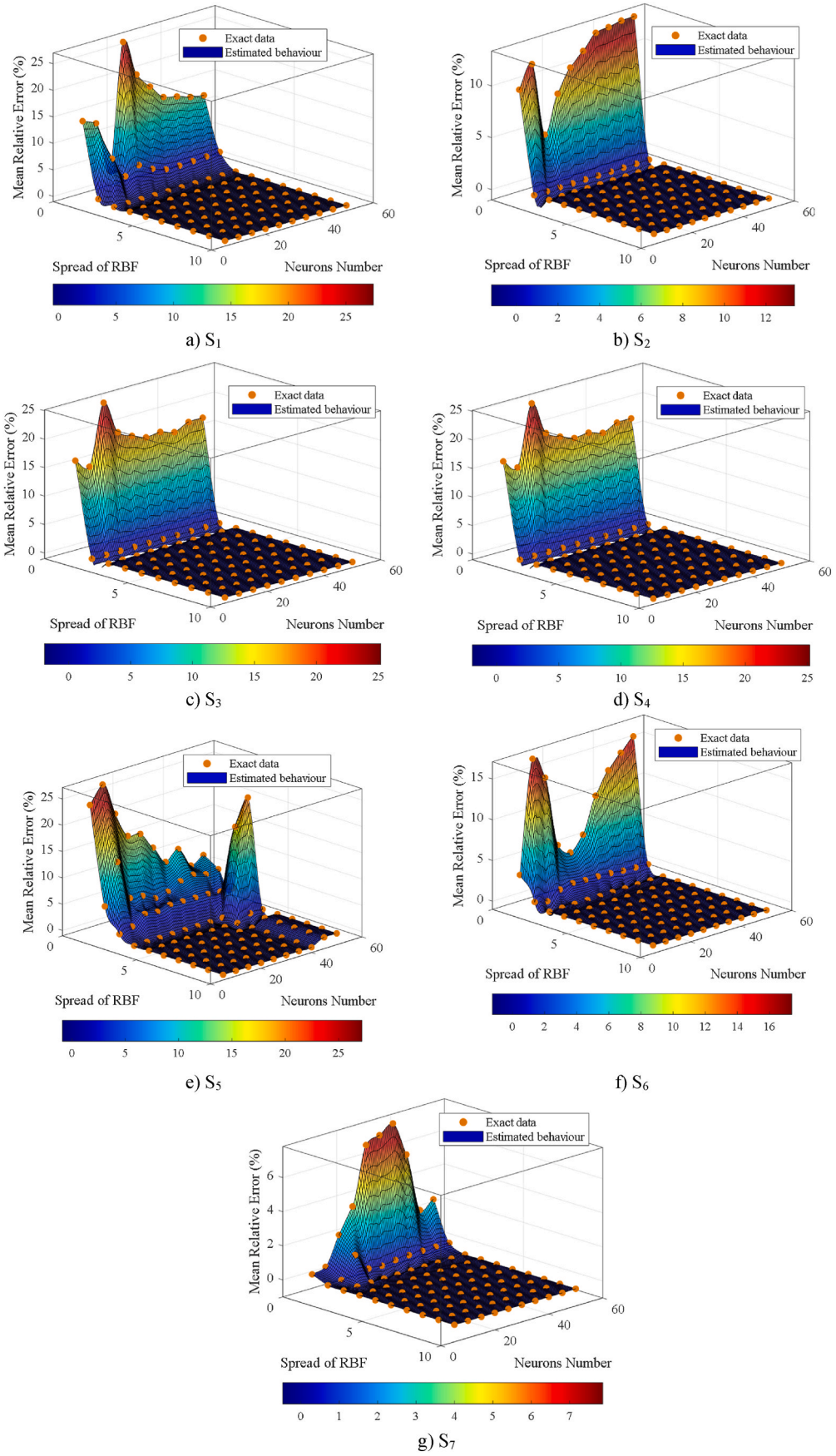

Fig. 8. The sensitivity analysis results after 50 times simulation repetition for different samples and different hyperparameters of RBFNN.

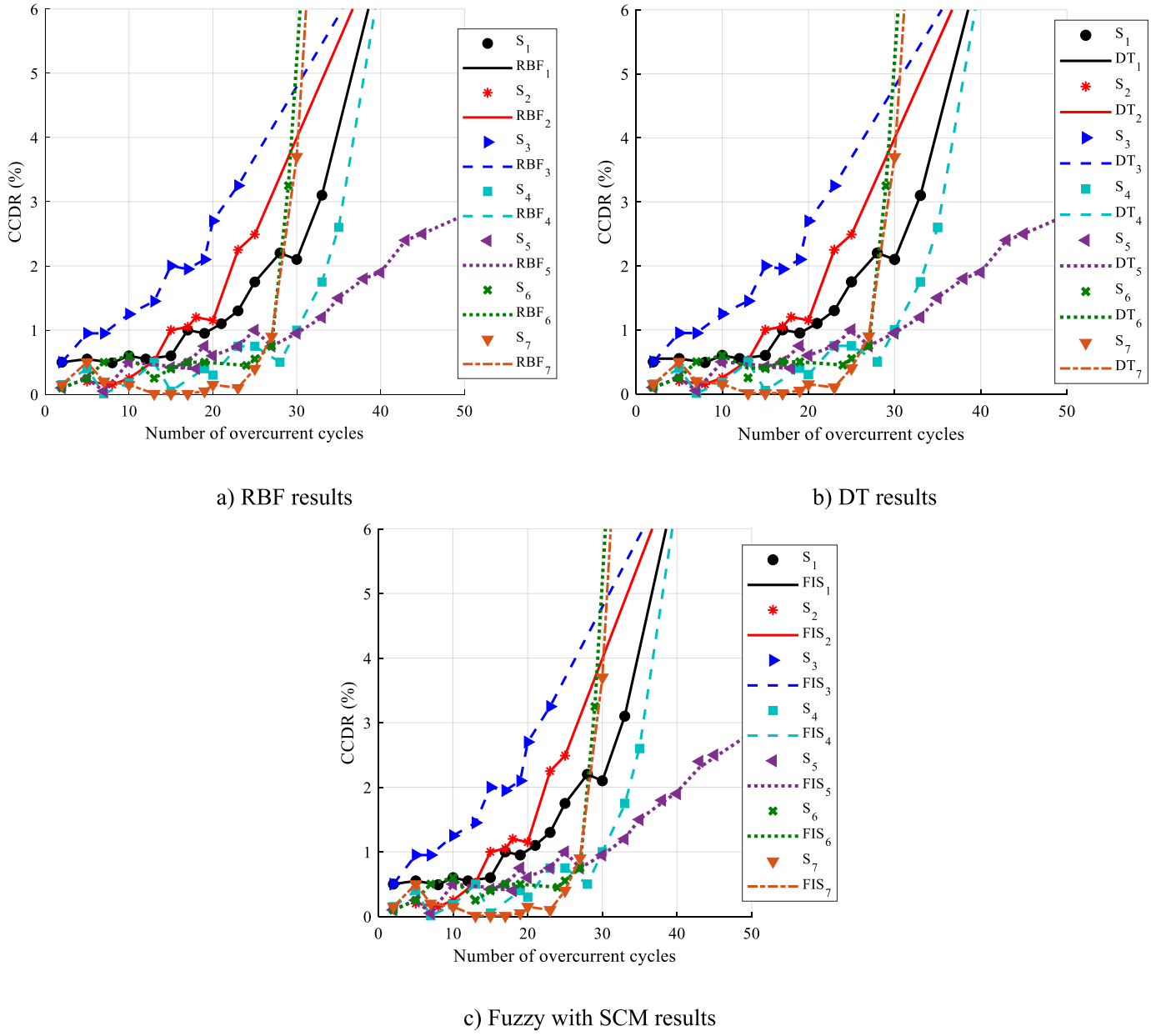

Fig. 9. Final estimation results versus real experimental data.

Table 11
Comparison of different estimation methods for CCDR.

Samples	RBFNN			DT			FIS		
	R	RMSE	MAC	R	RMSE	MAC	R	RMSE	MAC
S_1	1.000	2.4e-12	99.999999	0.9999	0.0129	99.998965	0.9999	1.5e-5	99.881
S_2	1.000	3.5e-11	99.999999	1.0000	1.2e-6	99.999999	0.9999	3.5e-4	96.474
S_3	1.000	9.6e-14	99.999999	1.0000	1.5e-5	99.999999	0.9999	2.2e-5	99.915
S_4	1.000	1.9e-13	99.999999	1.0000	9.2e-6	99.999999	0.9999	8.7e-3	82.210
S_5	0.999	9.4e-11	99.999999	1.0000	5.8e-6	99.999999	0.9993	5.2e-2	87.30
S_6	1.000	2.1e-13	99.999999	0.9999	0.0416	99.996541	0.9999	4.9e-6	99.999
S_7	0.999	1.3e-12	99.999999	1.0000	1e-7	99.999999	0.9999	3.5e-5	91.712

4. Conclusion

Overcurrent events are one of significant factors contributing to the partial or fully degradation of the critical current in High Temperature Superconducting (HTS) tapes. The degradation of critical current could reduce the reliability and remaining life of HTS devices. In the existing literature, experimental tests have been conducted to measure the Critical Current Degradation Rate (CCDR) of HTS tapes, and analytical methods have been employed to estimate the trends in the experimental data. This paper proposes Artificial Intelligence (AI) techniques to

Table 12
Estimation comparison of proposed methods with methods published in literature and fitting methods.

Method	MRE (%)	RMSE (%)
LPM [7]	8.2	0.1487
SBM [7]	8.4	0.1589
F_1 (linear)	50.2	1.6905
F_2 (3rd order Polynomial)	8.1	0.1572
F_3 (exponential)	10.1	0.3969
RBFNN	1.1×10^{-6}	2e-12
DT	0.06	0.0129
FIS	0.61	4.9e-6

address the low accuracy of existing estimation methods. The proposed AI techniques are investigated by Support Vector Regression (SVR), Radial Basis Function Neural Network (RBFNN), Decision Tree (DT), and Fuzzy Inference Systems (FIS). The main findings of this work are:

- In DT model, the increase in the number of trees, resulted in accuracy enhancement and training/testing times increased.
- The selected structure for DT model is when 30 trees are considered that results in Mean Relative Error (MRE) lower than 1% with about 1 s of train time and a test time of 10 ms.
- The MRE of best FIS model is lower than 0.2% while train and test times are 638 ms and 9.95 ms, respectively.
- The SVR method for all cases has high error which make it impractical for CCDR estimation.
- RBFNN model has the best performance when spread value is higher than 5 with number of neurons higher than 30 that results in MRE well lower than 1e-6%.
- The MRE of AI-based methods proposed in this paper, such as FIS, DT, and RBFNN is 100x to 1000x lower compared to data-driven-based methods, presented in literature.

CRediT authorship contribution statement

Alireza Sadeghi: Writing – original draft, Visualization, Software, Methodology, Investigation, Formal analysis, Data curation, Conceptualization. **Shahin Alipour Bonab:** Visualization, Software, Data curation. **Wenjuan Song:** Writing – review & editing, Validation, Resources, Investigation, Funding acquisition, Conceptualization. **Mohammad Yazdani-Asrami:** Writing – review & editing, Validation, Supervision, Resources, Project administration, Methodology, Investigation, Conceptualization, Formal analysis, Writing – original draft.

Declaration of competing interest

The authors declare that they have no known competing financial interests or personal relationships that could have appeared to influence the work reported in this paper.

Data availability

Data will be made available on request.

Acknowledgments

For the purpose of open access, the author(s) has applied a Creative Commons Attribution (CC BY) license to any Author Accepted Manuscript version arising from this submission.

This work was supported by the U.K. Engineering and Physical Sciences Research Council (EPSRC) under Grant EP/X5257161/1.

References

[1] E. Papadis, G. Tsatsaronis, Challenges in the decarbonization of the energy sector, Energy 205 (Aug. 2020): 118025, https://doi.org/10.1016/j.energy.2020.118025.
[2] C.A. Luongo, et al., Next generation more-electric aircraft: a potential application for HTS superconductors, IEEE Trans. Appl. Supercond. 19 (3) (Jun. 2009) 1055–1068, https://doi.org/10.1109/TASC.2009.2019021.
[3] M. Yazdani-Asrami, S. Seyyedbarzegar, A. Sadeghi, W.T.B. de Sousa, D. Kottonau, High temperature superconducting cables and their performance against short circuit faults: current development, challenges, solutions, and future trends, Supercond. Sci. Technol. 35 (8) (Aug. 2022): 083002, https://doi.org/10.1088/1361-6668/ac7ae2.
[4] G. Chen, et al., Critical current degradation behavior of coated conductor subjected to repeat overcurrent, IEEE Trans. Appl. Supercond. 30 (4) (Jun. 2020) 1–6, https://doi.org/10.1109/TASC.2020.2967683.
[5] A. Ishiyama, et al., Degradation characteristics of REBCO-coated conductors subjected to overcurrent pulse, IEEE Trans. Appl. Supercond. 19 (3) (Jun. 2009) 3483–3486, https://doi.org/10.1109/TASC.2009.2018734.
[6] A. Ishiyama, et al., Degradation of REBCO coated conductors due to over-current pulse, IEEE Trans. Appl. Supercond. 17 (2) (Jun. 2007) 3509–3512, https://doi.org/10.1109/TASC.2007.899708.
[7] X. Ding, et al., Research on data-driven approaches for life prediction of REBCO Tapes under overcurrent, IEEE Trans. Appl. Supercond. 33 (3) (Apr. 2023) 1–10, https://doi.org/10.1109/TASC.2022.3230798.
[8] S. Yazaki, A. Karasawa, T. Kotoyori, A. Ishiyama, N. Miyahara, Critical current degradation in high-temperature superconducting Tapes caused by temperature rise, IEEE Trans. Appl. Supercond. 23 (3) (Jun. 2013): 4602304, https://doi.org/10.1109/TASC.2013.2244157. –4602304.
[9] W. Chen, et al., Fatigue behavior of critical current degradation for REBCO Tapes at 77 K, IEEE Trans. Appl. Supercond. 28 (3) (Apr. 2018) 1–5, https://doi.org/10.1109/TASC.2018.2806912.
[10] H.-S. Shin, J.R.C. Dizon, T.-H. Kim, D.-W. Ha, S.-S. Oh, Critical current degradation behavior in REBCO coated conductors under torsional strain, IEEE Trans. Appl. Supercond. 17 (2) (Jun. 2007) 3274–3277, https://doi.org/10.1109/TASC.2007.897458.
[11] Y. Xu, et al., Critical current degradation of REBCO tape with different stabilizing layers under cyclic mechanical strains, IEEE Trans. Appl. Supercond. 30 (4) (Jun. 2020) 1–7, https://doi.org/10.1109/TASC.2020.2970386.
[12] H.-S. Shin, K.-H. Kim, J.R.C. Dizon, T.-Y. Kim, R.-K. Ko, S.-S. Oh, The strain effect on critical current in REBCO coated conductors with different stabilizing layers, Supercond. Sci. Technol. 18 (12) (Dec. 2005) S364–S368, https://doi.org/10.1088/0953-2048/18/12/023.
[13] K.H. Jensen, et al., Overcurrent experiments on HTS tape and cable conductor, IEEE Trans. Appl. Supercond. 11 (1) (Mar. 2001) 1781–1784, https://doi.org/10.1109/77.920130.
[14] J.W. Lue, M.J. Gouge, R.C. Duckworth, Over-current testing of HTS Tapes, IEEE Trans. Appl. Supercond. 15 (2) (Jun. 2005) 1835–1838, https://doi.org/10.1109/TASC.2005.849306.
[15] G. Chen, et al., Failure analysis of REBCO Tapes considering the amplitude and duration of sinusoidal overcurrent, IEEE Trans. Appl. Supercond. 29 (5) (Aug. 2019) 1–5, https://doi.org/10.1109/TASC.2019.2897374.
[16] Gang Zhou Yi, Guo Min Zhang, Hang Li Xiao, Ying Shun Wang, Zhen Lin Liang, Li Ye Xiao, Performance of REBCO Tapes with different structures under AC overcurrent conditions, IEEE Trans. Appl. Supercond. 19 (4) (Aug. 2009) 3665–3669, https://doi.org/10.1109/TASC.2009.2019627.
[17] H. Kono, et al., Degradation characteristics of REBCO coated conductors due to fault-current in power cable applications, Phys. C: Supercond. Appl. 470 (20) (Nov. 2010) 1334–1337, https://doi.org/10.1016/j.physc.2010.05.106.
[18] Xudong Wang, Tao Wang, A. Ishiyama, M. Yagi, O. Maruyama, T. Ohkuma, Experiments and numerical simulations on local degradation characteristics of coated conductor due to overcurrent, IEEE Trans. Appl. Supercond. 23 (3) (Jun. 2013) 8002205, https://doi.org/10.1109/TASC.2013.2238592, 8002205.
[19] J. Sheng, H. Sun, X. Liu, Z. Jin, Z. Hong, Performance degradation of YBa2Cu3O7-δ tapes after suffering lightning impulse current, Appl. Phys. Lett. 104 (11) (Mar. 2014), https://doi.org/10.1063/1.4868639.
[20] G. Wu, H. Yong, Estimation of critical current density of bulk superconductor with artificial neural network, Superconductivity 7 (Sep. 2023): 100055, https://doi.org/10.1016/j.supcon.2023.100055.
[21] M. Yazdani-Asrami, L. Fang, X. Pei, W. Song, Smart fault detection of HTS coils using artificial intelligence techniques for large-scale superconducting electric transport applications, Supercond. Sci. Technol. 36 (8) (Aug. 2023): 085021, https://doi.org/10.1088/1361-6668/ace3fb.
[22] M. Yazdani-Asrami, Artificial intelligence, machine learning, deep learning, and big data techniques for the advancements of superconducting technology: a road to smarter and intelligent superconductivity, Supercond. Sci. Technol. 36 (8) (Aug. 2023): 084001, https://doi.org/10.1088/1361-6668/ace385.
[23] M. Yazdani-Asrami, et al., Roadmap on artificial intelligence and big data techniques for superconductivity, Supercond. Sci. Technol. 36 (4) (Apr. 2023): 043501, https://doi.org/10.1088/1361-6668/acbb34.
[24] G. Russo, M. Yazdani-Asrami, R. Scheda, A. Morandi, S. Diciotti, Artificial intelligence-based models for reconstructing the critical current and index-value surfaces of HTS tapes, Supercond. Sci. Technol. 35 (12) (Dec. 2022): 124002, https://doi.org/10.1088/1361-6668/ac95d6.
[25] W.A. Belson, Matching and prediction on the principle of biological classification, Appl Stat 8 (2) (Jun. 1959) 65, https://doi.org/10.2307/2985543.

[26] B. de Ville, Decision trees, WIREs Comput. Stat. 5 (6) (Nov. 2013) 448–455, https://doi.org/10.1002/wics.1278.
[27] S.B. Kotsiantis, Decision trees: a recent overview, Artif. Intell. Rev. 39 (4) (Apr. 2013) 261–283, https://doi.org/10.1007/s10462-011-9272-4.
[28] B. Charbuty, A. Abdulazeez, Classification based on decision tree algorithm for machine learning, J. Appl. Sci. Technol. Trends 2 (1) (Mar. 2021) 20–28, https://doi.org/10.38094/jastt20165.
[29] I.D. Mienye, Y. Sun, Z. Wang, Prediction performance of improved decision tree-based algorithms: a review, Procedia Manuf. 35 (2019) 698–703, https://doi.org/10.1016/j.promfg.2019.06.011.
[30] M. Somvanshi, P. Chavan, S. Tambade, S.V. Shinde, A review of machine learning techniques using decision tree and support vector machine, in: 2016 International Conference on Computing Communication Control and Automation (ICCUBEA), IEEE, Aug. 2016, pp. 1–7, https://doi.org/10.1109/ICCUBEA.2016.7860040.
[31] E. Pekel, Estimation of soil moisture using decision tree regression, Theor. Appl. Climatol. 139 (3–4) (Feb. 2020) 1111–1119, https://doi.org/10.1007/s00704-019-03048-8.
[32] L.A. Zadeh, Fuzzy sets, Inf. Control 8 (3) (Jun. 1965) 338–353, https://doi.org/10.1016/S0019-9958(65)90241-X.
[33] L. Jouffe, Fuzzy inference system learning by reinforcement methods, IEEE Trans. Syst. Man and Cybern. Part C (Appl. Rev.) 28 (3) (1998) 338–355, https://doi.org/10.1109/5326.704563.
[34] N. Varma Ulchi Suresh, A. Sadeghi, M. Yazdani-Asrami, Critical current parameterization of high temperature Superconducting Tapes: a novel approach based on fuzzy logic, Superconductivity 5 (Mar. 2023): 100036, https://doi.org/10.1016/j.supcon.2023.100036.
[35] C.C. Lee, Fuzzy logic in control systems: fuzzy logic controller, IEEE Trans Syst Man Cybern 20 (2) (1990) 408–414, https://doi.org/10.1109/21.52551.
[36] M. Yazdani-Asrami, A. Sadeghi, S.M. Seyyedbarzegar, A. Saadat, Advanced experimental-based data-driven model for the electromechanical behavior of twisted REBCO tapes considering thermomagnetic constraints, Supercond. Sci. Technol. 35 (5) (2022): 054004, https://doi.org/10.1088/1361-6668/ac57be.
[37] J. Serrano-Guerrero, F.P. Romero, J.A. Olivas, Fuzzy logic applied to opinion mining: a review, Knowl. Base Syst. 222 (Jun. 2021): 107018, https://doi.org/10.1016/j.knosys.2021.107018.
[38] K. Mittal, A. Jain, K.S. Vaisla, O. Castillo, J. Kacprzyk, A comprehensive review on type 2 fuzzy logic applications: past, present and future, Eng. Appl. Artif. Intell. 95 (Oct. 2020): 103916, https://doi.org/10.1016/j.engappai.2020.103916.
[39] A. Azadegan, L. Porobic, S. Ghazinoory, P. Samouei, A. Saman Kheirkhah, Fuzzy logic in manufacturing: a review of literature and a specialized application, Int. J. Prod. Econ. 132 (2) (Aug. 2011) 258–270, https://doi.org/10.1016/j.ijpe.2011.04.018.
[40] J.M. Mendel, Fuzzy logic systems for engineering: a tutorial, Proc. IEEE 83 (3) (Mar. 1995) 345–377, https://doi.org/10.1109/5.364485.
[41] D.A. Pisner, D.M. Schnyer, Support vector machine, in: Machine Learning, Elsevier, 2020, pp. 101–121, https://doi.org/10.1016/B978-0-12-815739-8.00006-7.
[42] S. Salcedo-Sanz, J.L. Rojo-Álvarez, M. Martínez-Ramón, G. Camps-Valls, Support vector machines in engineering: an overview, WIREs Data Min. Knowl. Discov. 4 (3) (May 2014) 234–267, https://doi.org/10.1002/widm.1125.
[43] W.S. Noble, What is a support vector machine? Nat. Biotechnol. 24 (12) (Dec. 2006) 1565–1567, https://doi.org/10.1038/nbt1206-1565.
[44] V.N. Vapnik, The Nature of Statistical Learning Theory, Springer, New York, 2000, https://doi.org/10.1007/978-1-4757-3264-1. New York, NY.
[45] C. Li, X. Mei, Application of SVR models built with AOA and Chaos mapping for predicting tunnel crown displacement induced by blasting excavation, Appl. Soft Comput. 147 (Nov. 2023): 110808, https://doi.org/10.1016/j.asoc.2023.110808.
[46] Bing Yu and Xingshi He, "Training Radial Basis Function Networks with Differential Evolution," in 2006 IEEE International Conference on Granular Computing, IEEE, pp. 369–372. doi: 10.1109/GRC.2006.1635817.].
[47] C. Zhanjian, et al., Proposing an intelligent technique based on radial basis function neural network to forecast the energy spectrum of diagnostic X-ray imaging systems, Appl. Radiat. Isot. 200 (Oct. 2023): 110961, https://doi.org/10.1016/j.apradiso.2023.110961.
[48] E.J. Hartman, J.D. Keeler, J.M. Kowalski, Layered neural networks with Gaussian hidden units as universal approximations, Neural Comput. 2 (2) (Jun. 1990) 210–215, https://doi.org/10.1162/neco.1990.2.2.210.
[49] K.L. Du, M.N.S. Swamy, Radial basis function networks, in: Neural Networks in a Softcomputing Framework, 2006, pp. 251–294.
[50] M. Yazdani-Asrami, et al., Artificial intelligence methods for applied superconductivity: material, design, manufacturing, testing, operation, and condition monitoring, Supercond. Sci. Technol. 35 (123001) (2022) 54, https://doi.org/10.1088/1361-6668/ac80d8.
[51] M. Yazdani-Asrami, A. Sadeghi, S. Seyyedbarzegar, W. Song, DC electro-magneto-mechanical characterization of 2G HTS Tapes for superconducting cable in magnet system using artificial neural networks, IEEE Trans. Appl. Supercond. 32 (7) (Oct. 2022) 1–10, https://doi.org/10.1109/TASC.2022.3193782.
[52] X. Ding, et al., Research on data-driven approaches for life prediction of REBCO Tapes under overcurrent, IEEE Trans. Appl. Supercond. 33 (3) (2023): 6600710.